

Baryons and tetraquarks using instanton-induced interactions

Nicholas Miesch,^{*} Edward Shuryak,[†] and Ismail Zahed[‡]
*Center for Nuclear Theory, Department of Physics and Astronomy,
 Stony Brook University, Stony Brook, New York 11794-3800, USA*

We analyze some aspects of the perturbative and non-perturbative interactions in the composition of heavy quarkonia, heavy and light baryons (ccc and uuu ones), as well as all charm tetraquarks ($cc\bar{c}\bar{c}$). Using the hyper-spherical approximation and effective radial potentials (in 6 and 9 dimensions, respectively) we derive their spectra and wave functions. In all of the cases, we focus on the splittings between the s-shell levels, which are remarkably insensitive to the quark masses, but proportional to the effective interaction potentials. We use the traditional Cornell-like potentials, and the non-perturbative instanton-induced static potentials, from correlators of two, three and four Wilson lines, and find rather satisfactory description of spectra in all cases.

I. INTRODUCTION

One of the goals of the present paper is to reassess the information one can extract from hadronic spectroscopy, on quark-quark and quark-antiquark interactions in multi-quark system, baryons and tetraquarks. Of course, we do not attempt to cover this vast field, but rather focus on some particular (flavor-symmetric) objects. Furthermore, we focus on specific features of spectroscopy that are most sensitive to the inter-quark interactions (and less sensitive to the quark masses and additive constants in the potentials).

As examples of these observables, we use the *splittings* between the $1S, 2S, 3S$ states (S-shell, as usual means zero angular momentum), and evaluate the splittings between the p-shell states (negative parity). We start in section II with a very traditional issue, in relation to the central quarkonium potential in charmonium and bottomonium. In spite of the large mass difference between c, b quarks, these splittings in are very similar. While this fact by itself is widely known, we elaborate in more detail on its sensitivity to the exact shape of the potentials. More specifically, we use comparatively the Cornell (Coulomb-plus-linear) potential, the Martin potential, and the instanton-induced potential we derived in [1] (our first paper of the light-front series) .

In sections II A and III A we discuss the flavor-symmetric baryons (ccc, uuu) and $cc\bar{c}\bar{c}$ tetraquarks, respectively. As a method, we use the so called *hyperdistance* (or hypercentral, or K-harmonics) ap-

proximation, by reducing quantum mechanics (in 6 dimensions for baryons and 9 for tetraquarks) to a single radial Schrodinger equation. The method has been developed in the 1960's, in nuclear physics, for the quantum mechanical treatment of light nuclei, see e.g. [2]. One well-known four-body example is 4He , for which this approach reproduces its binding $\approx 28 MeV$ from conventional nuclear forces. Furthermore, in a relatively recent paper [3] on 4-nucleon clustering in heavy ion collisions at finite temperatures, it was found that the same hyperdistance equation also correctly predicts the *second* ($2S$) level of 4He , with small binding and close to its experimentally known location. This work increased our trust in this approach, at least for the splittings of the s-shell states.

The applications of the hyperdistance approximation to various multiquark states have also been done over the years, see e.g. [4–8] and references therein. With the recent revival of hadronic spectroscopy due to the discovery of multiple tetra- and penta-quark states, there has been renewed interest in few-body quantum mechanics in general, and in the hyperdistance approximation in particular.

In sections III A and C, we start our analyses using Cornell-like potentials, and focus chiefly on the level splittings of the S-shell states. Much like in quarkonia, we found that the splittings are insensitive to the quark mass values: for ccc and uuu baryons, these splittings are nearly identical, see Fig.3. What they are sensitive to is the overall strength of the confining force in multiquark systems, to which they are roughly proportional. (This is highly nontrivial, since the wave functions and even sizes of these systems are vastly different!)

The main physics issues this paper is aimed at are the following questions: Can the interactions inside

^{*} nicholas.miesch@stonybrook.edu

[†] edward.shuryak@stonybrook.edu

[‡] ismail.zahed@stonybrook.edu

few-body hadrons (such as baryons and tetraquarks specifically) be approximated by a sum of two-body ones? Do they only depend on the *hyper-distance* variable (related to the sum of distances between all constituents squared)? If so, are the shapes of the corresponding effective potentials similar to the Coulomb+linear potentials used for quarkonia? What are the magnitude of their respective coefficients, for 3 and 4 quarks? What is the order of magnitude of the corrections stemming from the lowest hyper-spherical approximation?

Static interquark potentials have well known expressions in terms of the correlators of Wilson lines. Lattice gauge theories in fact started with the evaluation of correlated Wilson lines $\langle WW^\dagger \rangle$, and the shape of the $\bar{q}q$ static potential. The literature on this subject is vast and cannot be covered in this work. Yet the lattice studies of correlators of three or four Wilson lines are surprisingly limited, with results limited to simple geometries for forces in baryons [9] and in tetraquarks [10]. For the baryons, three quarks are set at the corners of triangles of different shapes and sizes, while for tetraquarks four quarks are set at the corners of rectangles $r \times R$ with variable r, R . Unfortunately, no attempts to project the results on the hyperdistance variable were made so far.

While numerical lattice simulations are first-principle-based approaches to vacuum ensemble of gauge fields, some simple models for the vacuum have been developed over the years. Instantons are 4-d spherical solutions in Euclidean gauge theory vacua, describing tunneling between configurations with different Chern-Simons numbers. They are the basis of semiclassical approximation and trans-series in QFT. Here, we will not go into the theoretical details of the model, but just state that we will use what we refer to as the "dense instanton vacuum model". Unlike earlier version, the "dilute instanton vacuum" [11] (which included only isolated instantons and focused on their fermionic zero modes and chiral symmetry breaking, for review see [12]), it also includes close instanton-antiinstanton pairs which contribute to Wilson lines by their fields. The two parameters of the model are the 4d density $n_{I+\bar{I}} \approx 7 \text{ fm}^{-4}$ of instantons and antiinstantons, and their mean size $\rho \approx \frac{1}{3} \text{ fm}$. For discussion of these parameters and its relation to static quarkonium potential see [1]. Throughout the same parameters will be used in the evaluation of the effective potentials in all systems considered, e.g. $\bar{q}q, qq\bar{q}, qq\bar{q}\bar{q}$. So the

resulting potentials are essentially parameter free. All we do is to generalize the calculation of Wilson line correlators $\langle WW^\dagger \rangle$, to WWW and $WWW^\dagger W^\dagger$ pertinent correlators. We are satisfied to find that the resulting potentials do indeed reproduce the pertinent hadron spectra in all cases.

II. CENTRAL POTENTIAL IN QUARKONIA

Since the early 1970's, when heavy c, b quarks were discovered, the nonrelativistic description of quarkonia $\bar{c}c, \bar{b}b$ states became the main pillars of hadronic spectroscopy. And yet, we decided to start again from quarkonia, to test how well the proposed potentials work.

A good motivation is to also include current data on bottomonium states, as listed in the review of particle physics 2022 [13]. We focus below on the S-level *splittings*, insensitive to quark masses and overall constant terms in the potentials. One such input is the splitting between the spin-averaged charmonium masses

$$M_{spin-average} = (3M_\psi + M_{\eta_c})/4 \quad (1)$$

in the 2S and 1S shell

$$M_{spin-average}^{2S} - M_{spin-average}^{1S} \approx 605 \text{ MeV} \quad (2)$$

In the bottomonium family we now have Υ states listed up to 4S, but not enough η_c states to perform spin average for all of them. Hence, we will use the Upsilon mass splittings instead. (Spin-dependent forces are not yet included, but those are $\sim 1/m_b^2$ and rather small in bottomonia.) These data points are shown as red pentagons in Fig.1.

The precise shape of static potential, describing known quarkonium masses, is an old problem, discussed many times since e.g. the first reviews such as [14]. The classic Cornell potential is the sum of the one-gluon exchange Coulomb term, and the linear confining term. For definiteness, we use its version with coefficients

$$V_{Cornell} = -\frac{0.641}{r} + 0.113 \cdot r \quad (3)$$

(Throughout, all dimensions are in GeV units, e.g. the distance r is in GeV^{-1} , and the string tension in GeV^2 .) The two parameters in the potential are fitted so as to reproduce the three known bottomonium splittings $2S - 1S, 3S - 1S, 4S - 1S$, shown

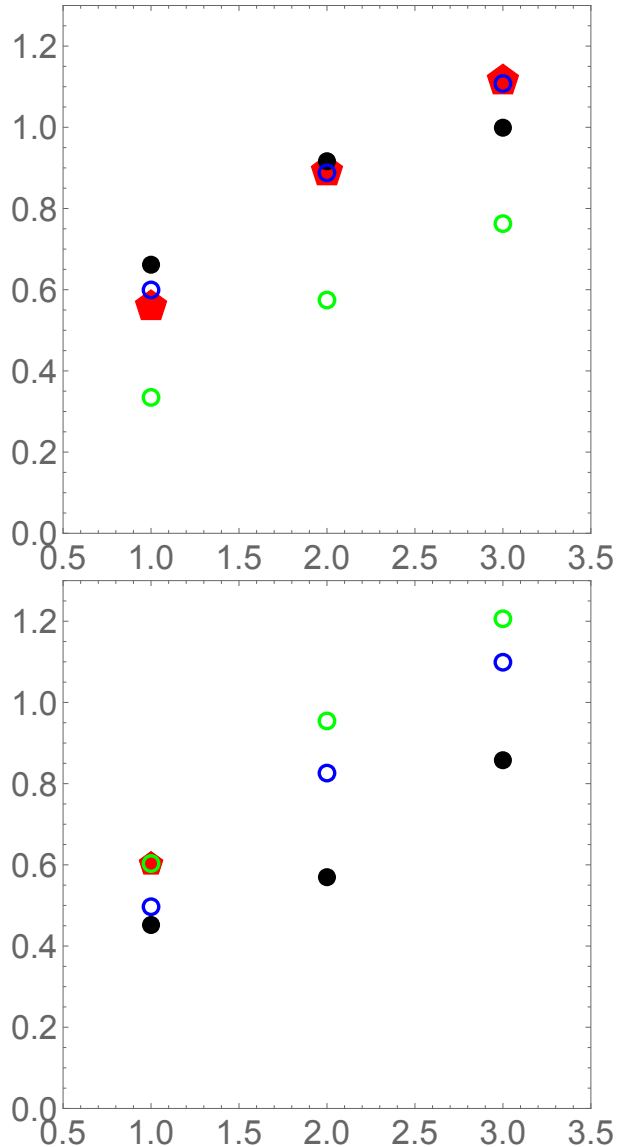


FIG. 1. Mass splittings in GeV, of the $\Upsilon(nS) - \Upsilon(1S)$, $n = 2, 3, 4$ (upper plots) and spin-averaged splittings in $\bar{c}c$ systems (lower plots) shown versus $n - 1$ by red pentagons. The blue circles correspond to solution of the Schrodinger equation using the Cornell potentials, the green circles are for the Martin potential, and the black disks are for the instanton-induced potential explained in the text.

in the upper plot by the blue circles. Note that it does not reproduce well the charmonium splittings as shown in the lower panel of Fig. 1.

Let us remind the reader that potentials which grow as smaller power of r , display a smaller growth of energy with n . (Only an oscillator $V \sim r^2$ has

$E_n \sim n$ linearly.) Early studies argued that static potentials $V \sim r^\alpha$ with $\alpha < 1$ can describe spectra better. The so called *Martin potential* fitted to (then available) data, see e.g. [14]

$$V_{Martin}(r) = -8.054 + 6.870 \cdot r^{0.1} \quad (4)$$

(all in GeV) has a very small power, and therefore is close to a logarithmic potential, for which it is known that the 1S-2S splittings of the charmonium and bottomonium systems would be equal. And indeed, they are almost the same. More specifically, the spin-weighted average (1S, 2S) masses are (3068.65, 3673.95) MeV for charmonium and (9444.9, 10017.2) MeV for bottomonium, so $M(2S) - M(1S) = (605.3, 572.3)$ MeV for $(c\bar{c}, b\bar{b})$.

As one can see from the lower panel of Fig.1, with the Martin potential predictions for splittings are shown by green circles, it indeed does give a very accurate number for the first charmonium splitting (to which the potential parameter was originally fitted). Yet its predictions for $\bar{b}b$ Upsilon states (upper plot) is rather far from the data points.

To summarize our preliminary discussion: the Cornell potential is still perhaps the best choice, reproducing well these particular observables both for $\bar{c}c$ and $\bar{b}b$ systems. The potentials with smaller power, such as the Martin potential, do fit charmonium data but are not very good for bottomonia.

A. Instanton-induced forces in mesons

Understanding the hadronic spectroscopy can be viewed as only a step towards the even more ambitious goal of understanding the structure of the (Euclidean) gauge fields in the *QCD vacuum*. It may be approximate and schematic, yet it allows for practical evaluation of all kinds of *non-local correlations functions* of nonperturbative gauge fields, without supercomputers. The static potentials are the non-local correlators of fields inside the Wilson lines, the path-ordered exponents of color fields.

Instantons are nontrivial gauge configurations, being the basis of the semiclassical theory. Their properties in the QCD vacuum, chiral symmetry breaking and physical effects on mesonic and baryonic point-to-point correlators were reviewed in [12]. Recent discussion including the role of instanton-antiinstanton configurations on the lattice and for effective potentials can be found in the first paper of this series [1].

The contribution of instantons to the quark potential is an old subject, pioneered by [15], but its practical application to central and spin-dependent forces between quarks attracted very little attention [5]. In our recent series of papers [1, 16, 17], a novel version of the instanton model was proposed for that. It incorporates lattice data on close instanton-antiinstanton pairs and was shown to generate the $\bar{q}q$ static potential which, while not confining per se, is close to the Cornell potential up to about 1 fm distances.

We then extended this model to calculation of the spin-dependent $\bar{q}q$ forces, and static quark-quark potentials in diquarks and baryons. Those can be expressed as Wilson lines, decorated by two field strengths. In the cases of spin-spin and tensor forces, those fields are gluo-magnetic. (Note that attributing confinement to gluo-electric flux tubes, one is faced with the problematic of the spin-dependent forces. Indeed, there is no place as such for magnetic fields, and the only contribution is via the Thomas' precession. The instantons are self-dual, with gluomagnetic and gluoelectric components being equal, and thus they do generate significant spin-dependent forces.)

We now briefly recall some general points in the derivation of the $\bar{q}q$ potentials. The Wilson lines go along the world-path of static charges along the Euclidean time. The produced W operators are unitary color matrices, describing rotations of quark color vectors by certain angles and in certain directions, around which these rotations are to be made. Let the 3-vectors representing distances from the quark locations $\vec{r}_i, i = 1 \dots N$ to the instanton center be $\vec{\gamma}_i = \vec{r}_i - \vec{y}$ (amusingly it acts as a *vertex* center). The color rotation angles are

$$\alpha_i = \pi \left(1 - \frac{\gamma_i}{\sqrt{\gamma_i^2 + \rho^2}} \right) \quad (5)$$

where ρ is the instanton size. Far from the instanton, $\gamma_i \gg \rho$, this angle vanishes. At the instanton center $\gamma_i = 0$, the angle is maximal $\alpha_i = \pi$. The $SU(2)$ part of the Wilson line can be expressed using Pauli (rather than Gell-Mann) matrices $\tau^A, A = 1, 2, 3$

$$\begin{aligned} \mathbf{W}_{lb}^a &= \exp(\pm i \vec{\tau} \cdot \vec{n}_l \alpha_l) \\ &= (\cos(\alpha_l) \hat{\mathbf{1}} - i(\vec{\tau} \cdot \vec{n}_l) \sin(\alpha_l))_b^a \end{aligned} \quad (6)$$

where the unit vectors are $n_i = \vec{\gamma}_i / \gamma_i$, and $a, b = 1, 2; l = 1 \dots N_q$. The third color is not affected by the instanton fields, so this 2×2 matrix should be

complemented trivially by the unit value in the third row.

The integral over (large) Euclidean time $\tau \in [-T/2, T/2]$ may include some number of instantons N_{inst} . Summing over N_{inst} leads to the exponentiation of the correlator. The exponent is extensive in the Euclidean time T times the potential

$$V(r) = n_{I+\bar{I}} \int d^3y \frac{1}{N_c} \text{Tr}(\hat{\mathbf{1}} - W(0)W^\dagger(\vec{r})) \quad (7)$$

For the plot of it see Fig.5 of [1]. Below these formulae will be generalized for 3 and 4 quark lines. These calculations can later be straightforwardly generalized to other multi-quark hadrons. We plan to calculate the spin-dependent forces in the same settings in forthcoming publications.

The instanton-induced potential together with the Coulomb term, can be put into the Schrodinger equation, to derive the quarkonium states. Let us now return to Fig.1 for the mass differences between the excited $2S, 3S, 4S$ states, from the $1S$ ground state of $\bar{b}b, \bar{c}c$ quarkonia. The splittings for the instanton-based potential are shown in Fig.1 by black discs. For the $2S-1S$ and $3S-1S$ splittings of bottomonia the results match the data quite well, and only for the $4S$ state they visibly deviate from the data, by about 10% or so. For charmonia this potential leads to smaller level splittings. Overall, its accuracy is in between the Cornell and Martin potentials. Note however, that unlike those, fitted to reproduce quarkonia levels, the instanton parameters (sizes and density) were *not fitted* to spectroscopy, the instanton density and mean size taken directly from lattice data about vacuum topology.

III. BARYONS: HYPER-SPHERICAL APPROXIMATION AND INSTANTON-INDUCED POTENTIAL

A. Baryons in hyperspherical approximation

We started this paper discussing heavy quarkonia, and we will end discussing full-charm tetraquarks. However, it is also natural to address heavy-quark baryons, ccc or bbb , and anything in between. Unfortunately, these hadrons still elude experiments, so we will also include calculations for baryons composed of light quarks. In doing so, we will assign the same flavor for all three quarks, i.e. $uuu = \Delta^{++}$ states. (There is not enough data on $sss = \Omega^-$ spectra.)

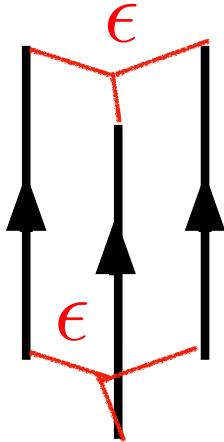


FIG. 2. Correlator of three Wilson lines in baryons, connected by a vertex with Levi-Cevita symbol.

We will use the *hyper-spherical approximation*, also known as the method of K-harmonics. The main idea is that the lowest states depend mostly on the radial hyperspherical coordinate in 6-d space of Jacobi coordinates

$$R_6^2 = \vec{\rho}^2 + \vec{\lambda}^2 \quad (8)$$

with a small admixture of components with angular dependences. In standard terms, we study 6-d s-shell states. Their wave function can be obtained by solving a single *radial* Schroedinger equation. The method has been used for baryons over the years, see e.g. [18] for heavy baryons of interest. The kinematical details of this approximation are given in Appendix A,B.

The radial Schrodinger equation for the S states has the form

$$\left(-u'' + \frac{15}{4R_6^2}u \right) \frac{1}{2M} + (V_6 - E_{Ns})u = 0 \quad (9)$$

where the reduced wave function $u(R_6)$ is related to the radial wave function by

$$\psi(R_6) = u(R_6)/R_6^{5/2} \quad (10)$$

Note, that R_6^5 gets absorbed in the volume element, so that u has the usual normalization, as in one dimension $\sim \int dR_6 |u(R_6)|^2$. This reduction eliminates the first derivative from the Laplacian, but adds an extra “quasi-centrifugal” term. The radial projection of the potential on R_6 is defined in the Appendix B.

The mass splittings of the lowest s- and p-states, ccc and uuu baryons, following numerically from (9) are shown in Fig.3. The binary QQ potential is taken as 1/2 of the Cornell potential (used above for Υ family). We do not show the absolute masses but focus instead on the level splittings. Experience shows that the splittings have relatively little dependence on the choice of the quark mass, but depend primarily on the interaction potential. Indeed, as shown in Fig.3, the plots for ccc and uuu baryons look nearly identical, in spite of the quark masses differing by more than a factor 3. (This is a reminder of the nearly identical splittings in the charmonium and bottomonium families emphasized above: those are also different by a similar ratio of 3 in absolute mass scale.)

More specifically, the splittings for the s-shell ccc baryons are calculated to be

$$M_{ccc}^{2S} - M_{ccc}^{1S} \approx 391, \quad M_{ccc}^{3S} - M_{ccc}^{1S} \approx 685 \text{ MeV}$$

and for the $uuu = \Delta^{++}$ states they are

$$M_{uuu}^{2S} - M_{uuu}^{1S} \approx 438, \quad M_{uuu}^{3S} - M_{uuu}^{1S} \approx 804 \text{ MeV}$$

The splittings for $uuu = \Delta(3/2^+)$ should be compared to experimental values of these splittings

$$M_{uuu}^{2S} - M_{uuu}^{1S} \approx 278, \quad M_{uuu}^{3S} - M_{uuu}^{1S} \approx 688 \text{ MeV},$$

(from the particle data tables 2022, using masses from the Breit-Wigner fits). While the deviations between the calculated and experimental values are comparable to the shifts expected from the spin-spin and 't Hooft forces, which are so far ignored in the calculation, its sign would be opposite, shifting 1S down more than higher states. (Also, these are relativistic corrections in $\sim 1/M^2$, and would of course be much less important for c quarks.) We therefore conclude that the effective potential for baryons used (Ansatz A), is somewhat stronger than it is in reality. We will elaborate on this point in the next section.

We also show the corresponding wave functions in Fig.4. Unlike the splittings, those show radical difference between the uuu and ccc baryons. Indeed, the corresponding hadrons are of quite different sizes, with the ccc ones much smaller. Also, all of them are somewhat unusual for the ground states. In spite of the enhanced Coulomb forces in the 6d systems, the quasi-centrifugal potential leads to wave functions very strongly suppressed at small hyper-radial distances.

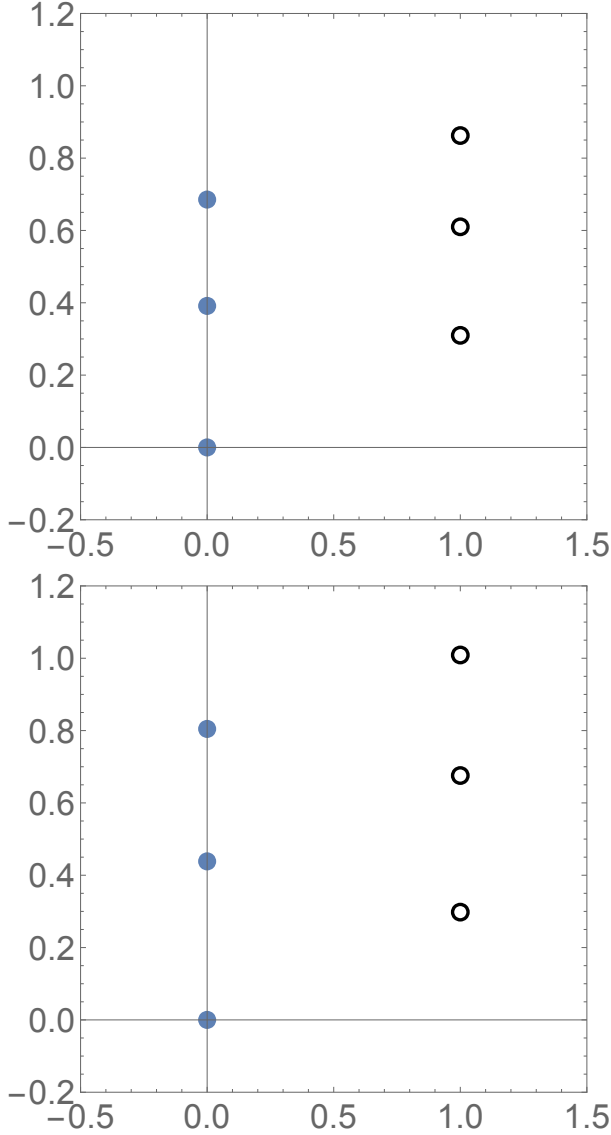


FIG. 3. Masses of ccc baryons (upper plot) and $uuu = \Delta^{++}$ (lower plot) $M(N, L)$, for $L = 0$ and $L = 1$ shells, counted from the ground states.

These wave functions can be used for getting matrix elements of various operators. R.m.s radii of three s-states of Δ are

$$\sqrt{\langle R_6^2 \rangle} = 4.97, 7.53, 9.72 \text{ GeV}^{-1} \quad (11)$$

To summarize this section: we have tested a popular assumption, that the non-perturbative forces between quarks in baryons can be described by a sum of binary forces reduced by the same factor $1/2$ (as perturbative ones), as compared to mesonic $\bar{Q}Q$ potential (the so called Ansatz A). We found that

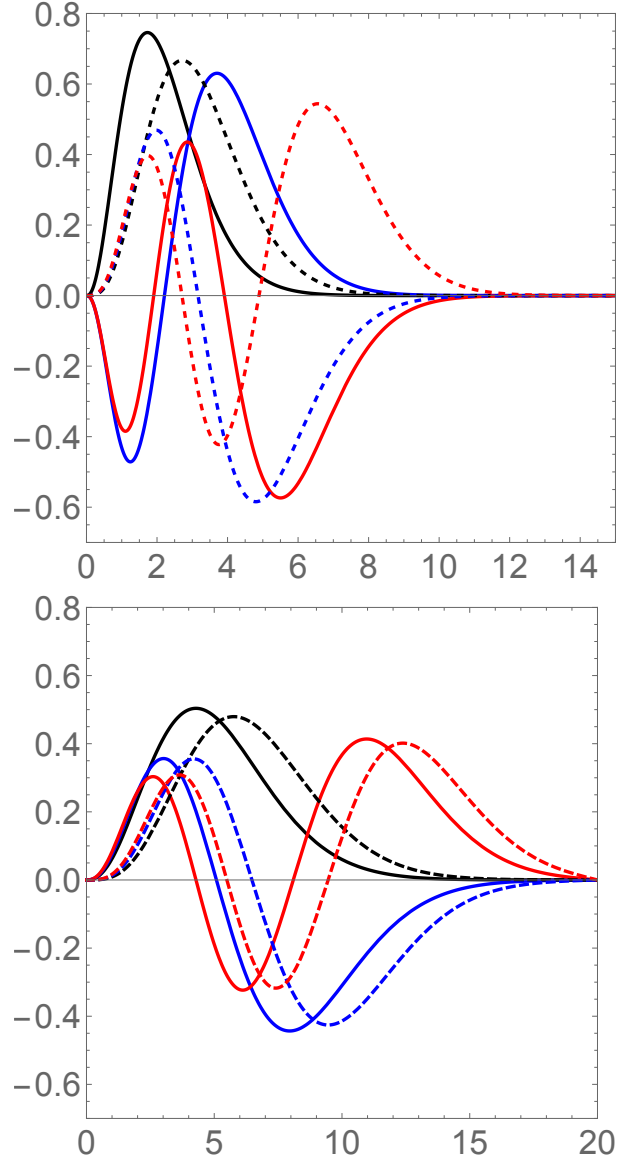


FIG. 4. Wave functions $u(R_6)$ of ccc (upper) and uuu baryons (lower) for $L = 0$ (solid lines) and $L = 1$ (dashed lines), versus the hyper-radial distance R_6 (GeV^{-1}).

it leads to splittings between s-shell states that are somewhat larger than observed in the $uuu = \Delta^{++}$ baryons. A possible fix is to introduce an arbitrary factor f for the confining force, and then fit it experimentally to the splittings if $f < 1/2$.

B. Instanton-induced potentials for baryons

We now derive the three-quark effective potential *along the radial 6d coordinate* $V_3(R_6)$, using the instanton model of the QCD vacuum.

We start by briefly recalling the approach we took in Ref.[16]. If no assumptions about the colors of the three quarks are made, the color indices of W remain open. Furthermore, to model a color-isotropic vacuum in which instantons are at random 2-d planes in the $SU(3)$ color space, we introduced random matrices $U \in SU(3)$ which rotate the instanton fields from their standard $SU(2)$ plane, $W \rightarrow UWU^\dagger$. All six matrices U were then averaged using the invariant *Haar measure* of the $SU(3)$ group,

$$\int dU (U_{i_1}^{a_1} \mathbf{W}_{1j_1}^{i_1} U_{b_1}^{\dagger j_1}) (U_{i_2}^{a_2} \mathbf{W}_{2j_2}^{i_2} U_{b_2}^{\dagger j_2}) (U_{i_3}^{a_3} \mathbf{W}_{3j_3}^{i_3} U_{b_3}^{\dagger j_3}) \quad (12)$$

before convolution of the external color indices. In [16] we used the so called 6- U "Weingarten formula" for this integral, and the Wilson lines running through instanton fields, leading to a "generic triple-quark potential" of the form

$$\begin{aligned} V = & n_{I+\bar{I}} \int d^3z \left[(1 - c_1 c_2 c_3) \delta_{b_1}^{a_1} \delta_{b_2}^{a_2} \delta_{b_3}^{a_3} \right. \\ & + \frac{9}{8} c_1 s_2 s_3 n_2 \cdot n_3 \delta_{b_1}^{a_1} \left(\frac{1}{2} \lambda_2^B \right)_{b_2}^{a_2} \left(\frac{1}{2} \lambda_3^B \right)_{b_3}^{a_3} \\ & \left. + 2 \text{perm.} \right] \quad (13) \end{aligned}$$

with trigonometric functions involving color rotation angles, that depend on the 3-dimensional distances $\tilde{\gamma}_i, i = 1, 2, 3$ between the location of the Wilson lines \vec{r}_i , and the instanton center \vec{y}

$$\begin{aligned} c_i & \equiv \cos(\alpha_i), \quad s_i \equiv \sin(\alpha_i) \\ \gamma_i^2 & = (\vec{r}_i - \vec{y})^2, \quad \vec{n}_i = \tilde{\gamma}_i / |\tilde{\gamma}_i| \end{aligned} \quad (14)$$

Since the standard instanton is an $SU(2)$ solution, it does not interact with a quark with the "third" color, orthogonal to the $SU(2)$ plane. The third color was ignored in the formula above. (Below we will extend the 2×2 matrix by adding $W_A(3, 3) = 1$ and other zeros to the 3×3 matrix.) Yet, for random orientations of the instanton induced by a rotation matrix U , and for arbitrary colors of the three quarks, the potential is generically a three-body potential, *not* a sum of two-body ones.

Here, we perform a different calculation, limiting it to the case of three quarks *making baryons*.

The corresponding color wave functions are $C_{ijk} = \epsilon_{ijk}/\sqrt{6}$. Putting those before and after the Wilson lines with the instanton-induced rotations (12), the result simplifies considerably. The randomizing matrices U acting on the Levi-Civita tensor cancel out (unit determinant). The resulting potential is therefore reduced to what we will call a "determinantal form"

$$\begin{aligned} V_3 = & (n_{I+\bar{I}} \rho^3) \int \frac{d^3y}{\rho^3} \quad (15) \\ & \times \left(1 - \sum \frac{\epsilon_{a_1 a_2 a_3}}{\sqrt{6}} W_1^{a_1 b_1} W_2^{a_2 b_2} W_3^{a_3 b_3} \frac{\epsilon_{b_1 b_2 b_3}}{\sqrt{6}} \right) \end{aligned}$$

Note that far from the instanton the color rotation angles of the Wilson lines (5) vanish. All $W_{ab} \rightarrow \delta_{ab}$ and therefore the integrand goes to zero, with a converging integral. Note also that we rewrote the integral over the instanton location d^3y as dimensionless, with a coefficient $(n_{I+\bar{I}} \rho^3) \approx 51 \text{ MeV}$.

Although this expression has the form of a generic three-body interaction of three Wilson lines, for Wilson lines in the field of an instanton, we (with some surprise) found that it does become the sum of three *binary* interactions for 12,13,23 pairs, each proportional to the "relative rotation"

$$\cos(\alpha_i) \cos(\alpha_j) + \sin(\alpha_i) \sin(\alpha_j) (\vec{n}_i \cdot \vec{n}_j) \quad (16)$$

The same combination appears in the $\bar{Q}Q$ potentials.

In Ref.[16] we evaluated the potential for different triangles, and compared the results to similar triangles studied on the lattice. Here we analyse baryons in the hyperspherical approximation, so we just take one equilateral triangle with variable size. The quarks are put at the locations $(r, 0, 0), (0, r, 0), (0, 0, r)$, so the distances between them are $r_{ij} = \sqrt{2}r$. Using the definitions of the Jacobi coordinates, one can see that $R_6 = \sqrt{2}r$ as well.

The effective three-quark potential V_3 in (15) for this equilateral triangle, is shown in Fig. 5. Here we used $n_{I+\bar{I}} = 7 \text{ fm}^{-4}, \rho = 1/3 \text{ fm}$, corresponding to the "dense instanton vacuum model" we used for the meson potential. Remarkably, the effective QQQ potential along R_6 , is quite similar in shape to the meson $Q\bar{Q}$ potential.

Using this potential (with the same one-gluon exchange as in previous section) in a hyperspherical approximation, gives the following splittings in the ccc and uuu baryons (GeV)

$$\begin{aligned} M_{ccc}^{2S} - M_{ccc}^{1S} & = 450, \quad M_{ccc}^{3S} - M_{ccc}^{1S} = 675, \text{ MeV} \\ M_{uuu}^{2S} - M_{uuu}^{1S} & = 232, \quad M_{uuu}^{3S} - M_{uuu}^{1S} = 394 \text{ MeV} \end{aligned}$$

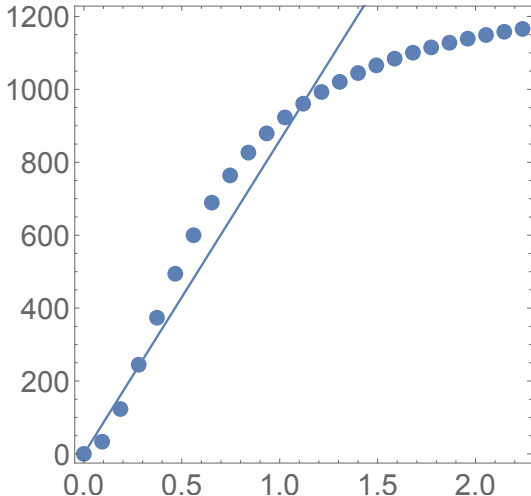


FIG. 5. The points show the instanton-induced effective potential in baryons $V(R_6)$, (MeV) vs R_6 (fm). The tension force is of the order of 1 GeV/fm (shown by a line for comparison).

While the results for the *ccc* baryons are very close to those found in the previous section for “ansatz A”, those for the *uuu* baryons are reduced significantly, and are now much closer to the experimental value of the first splitting. This means that the instanton-induced potential is a better representation of the force at $R_6 \sim 1$ fm. The splitting of the 3S state is too small because the instanton-induced potential at $R_6 > 1$ fm is flat. In order to get it in agreement with the data one would need a potential in between linear and constant, perhaps growing as a slower function of the distance.

IV. THE ALL-CHARM TETRAQUARKS

A. Masses and models

Experimentally these type of tetraquarks have been discovered by LHCb [19] and then by CMS [20] and ATLAS [21] in J/ψ , J/ψ and related channels. These states are named X(6550), X(6900), X(7280). For definiteness, we will use the ATLAS masses

$$M_1 = 6620, \quad M_2 = 6870, \quad M_3 = 7220 \text{ (MeV)} \quad (17)$$

all with errors ± 30 MeV. These states provide a good opportunity to check our understanding of both the multi-particle dynamics and inter-quark forces.

Among the many models put forth for the tetraquarks, we note the diquark-antidiquark formulation [22, 23], in which a 4-quark system is represented as a binary state of diquarks with binary potentials, equal to that in quarkonium $\bar{Q}Q$. This would be true if distances between quarks in diquarks (to be called r below) are much smaller than distances between diquarks R .

Since they are supposed to be comparable for $r \sim R$ in the lowest tetraquark states, we cannot neglect any of the 6 pair-wise interactions in the four-body compounds. In this section we use the four-body approach, with all six binary potentials included. Lattice studies of four-quark static potentials, with quenched and dynamical quarks, have been performed in [10]. (Again, the dependence on the hyper-distance could be determined, but was not.)

B. The lowest all-charm tetraquark states in the hyper-distance approximation

The use of the hyper-distance approximation for all-charm tetraquarks was pioneered in [4] (see also the recent study in [24]). The main idea is that for the lowest states, one may assume that they are mostly $L = 0$ s-shell, with only a small d-shell admixture. If so, we only need to solve a one-dimensional radial Schroedinger equation.

For four particles, there are three Jacobi coordinates, or 9-dimensions. We note that in our definition of these coordinates and hyper-distance (see Appendix D 1), as well as the ensuing radial equation, we differ with [24]. Also, our 9-dimensional wave function is written with a different power

$$\psi(R_9) = u(R_9)/R_9^4 \quad (18)$$

which allows the elimination of the first derivative term in the 9-d Laplacian, and also puts the normalization into the 1-dimensional form $\sim \int dR_9 |u(R_9)|^2$. The corresponding radial Hamiltonian is then

$$\left(-\frac{d^2}{dR_9^2} + \frac{12}{R_9^2} \right) \frac{1}{2M} + (4M + V) \quad (19)$$

in which the second term in the bracket is another “quasi-centrifugal” term, following from the 9-dimensional Laplacian.

The potential includes the color factors derived in Appendix D 1, which happen to be the same for $\bar{3}\bar{3}$

and $6\bar{6}$ diquark color structures. The other factors stemming from the angular projection of the inter-particle distances r_{ij} to the hyper-distance R_9 , are discussed in Appendix D 1 for the Cornell-type potentials. Here we use the Cornell potential as used for the Upsilon's above, with

$$V = 2 * (0.773 * R_9 * 0.113 - 1.55 * 0.64/R_9) \quad (20)$$

As for the mesons and baryons we discussed above, and in order not to get bogged down by the issue of the quark mass value and the constant in the potentials, we focus on the level *splittings*. Solving the Schroedinger equation (19), we find for the of the s-shell splittings

$$\begin{aligned} M(2S) - M(1S) &\approx 370 \text{ MeV} \\ M(3S) - M(1S) &\approx 689 \text{ MeV} \\ M(4S) - M(1S) &\approx 975 \text{ MeV} \end{aligned} \quad (21)$$

and for the p-shell splittings

$$\begin{aligned} M(1P) - M(1S) &\approx 587 \text{ MeV} \\ M(2P) - M(1S) &\approx 879 \text{ MeV} \end{aligned} \quad (22)$$

although the latters are not good candidate states for decaying into J/ψ pair.

From experimentally reported (ATLAS fit) masses of the three $cc\bar{c}\bar{c}$ resonances, we find for the splittings

$$\begin{aligned} M(2) - M(1) &\approx 250 \text{ MeV} \\ M(3) - M(1) &\approx 600 \text{ MeV} \end{aligned} \quad (23)$$

They are in fair agreement with the S-shell levels we calculated. As experience shows, this means that the overall magnitude of the forces in all the 6 quark pairs, is in reasonable agreement with the reported observations.

The corresponding wave functions are shown in Fig. 6. We note again, the very strong suppression at small hyper-distance, which is due to the quasi-centrifugal term in the Laplacian. (In [24] it is noted that it coincides with the centrifugal term for the $L = 3$ or F-shell quarkonia.) The r.m.s. sizes of these states are therefore rather large in GeV^{-1} , respectively.

V. INSTANTON-INDUCED FORCES IN TETRAQUARKS

The problem with the correlators of four Wilson lines, like for three ones, can either be set for (i)

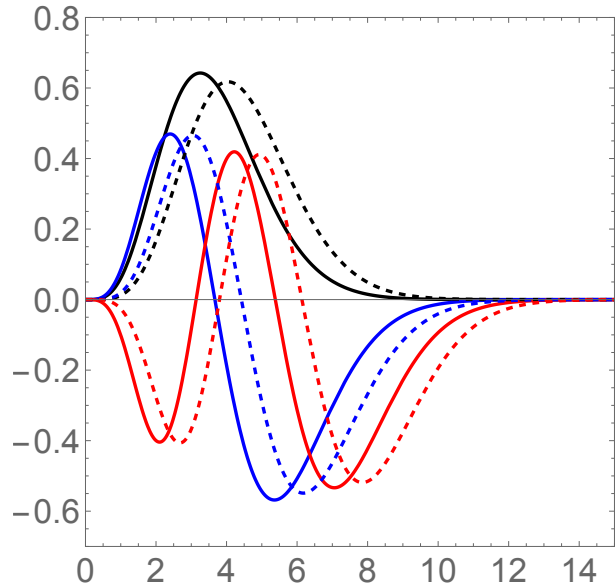


FIG. 6. The wave functions $u(\rho)$ for 1S,2S,3S states of all-charm tetraquarks in hyperspherical approximation, shown by solid black, blue and red lines, respectively. The dashed lines are p-shell states.

arbitrary colors of the quarks, or (ii) for those in a particular color wave function. In the former case, the correlator has color indices open and each Wilson line is rotated by random matrices UWU^\dagger , with subsequent averaging over the U using the invariant measure of the $SU(3)$ group. The general case of eight U is not used, but still discussed in Appendix E.

The color wave functions built from diquarks are discussed in Appendix D 1. Applying those at early and late times, we get certain products of delta indices. The convolution of the color indices is shown by red lines in Fig.7. The analytic expression for the $\bar{3}3$ correlator is

$$\begin{aligned} K_{\bar{3}3}(r, R) = & \quad (24) \\ & \left\langle \sum_{\bar{3}3} C_{\bar{3}3}^{c'_1, c'_2, c'_3, c'_4} W_{c'_1}^{c_1} W_{c'_2}^{c_2} W_{c'_3}^{c_3} W_{c'_4}^{c_4} C_{\bar{3}3, c_1, c_2, c_3, c_4} \right\rangle_y \end{aligned}$$

where the color wave functions are given in (D4). The sum is assumed over all color indices, and the averaging corresponds to the 3-dimensional integration over the instanton center position \vec{y} . Note that the anti-quark W (assumed here to be 3,4) are shown as transposed, yet by including the opposite color charges this is equivalent to Hermitian transposition of the corresponding unitary matrices. In effect, the

correlator corresponds to matrix products in the order indicated in Fig. 7. The same expression with the sextet wave-function is used for the $6\bar{6}$ correlator.

Although the diquarks on which the classification is based are pairs of qq or $\bar{q}\bar{q}$, the delta function connectors are between quarks and antiquarks, like in mesonic case. Therefore, the resulting structures consists of product of two traces (upper row) or a single trace (lower row) of Wilson lines products. Like in the baryon case, these traces do not change if W are all rotated by some matrices U . Again there is no need to use $SU(3)$ averaging of U (via Weingarten-style formulae).

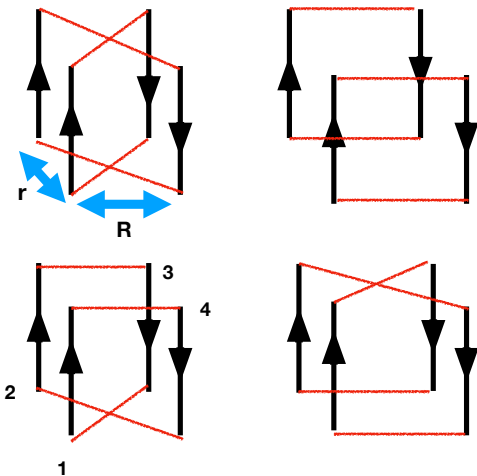


FIG. 7. The correlators of four Wilson lines in tetraquarks, connected according to the product of color wave-functions (D4) at times $\pm T$. The arrow directions show quarks (1 and 2) and antiquarks (3,4). In the $\bar{3}3$ case the convolutions in the second row appears with the minus sign, and in the $6\bar{6}$ case all terms have plus sign.

While four W can be located arbitrarily, we have only calculated the instanton contributions to correlators of four Wilson lines, placed at the corners of a $r \times R$ rectangle. The quarks are set to be 1,2 at distance r from each other, and the distance between the diquark and the antidiquark is set to be R . The potential, as usual, is defined as

$$V_{\bar{3}3}(r, R) = n_{I+\bar{I}} \int d^3y \left(1 - K_{\bar{3}3}(r, R) \right) \quad (25)$$

where, we recall that the calculation is basically the 3-dimensional integration over the location of the instanton center \vec{y} . For the $6\bar{6}$ case, the same formula applies, with the pertinent color wave-function. In

Fig. 8 we show only the results for the potential, from the symmetric “square setting” of charges, $r = R = R_9/\sqrt{2}$, its dependence on the overall size of the tetraquark, or the hyper-distance in 9 dimensions.

A key question is whether the $\bar{3}3$ and $6\bar{6}$ channels, support the same effective radial potentials. Our results in Fig.8, show that $6\bar{6}$ and $\bar{3}3$ potentials are not identical. An inherent repulsion in the $6\bar{6}$ channel generates an extra increase in the potential, especially at large $R_9 > 1 fm$. We conclude that the instanton-based forces *approximately* support equality of the potentials in both channels, as anticipated in [4].

As in all similar calculations at small $R_9 \rightarrow 0$, the strong cancellations between the quark and antiquark contributions, lead to a vanishing effective potential. The overall shape of the potential is similar (but not equal) to other instanton-induced potentials (e.g. qqq one in Fig.5).

At large distances, the potentials tend to constants, since the instanton vacuum does not confine. However, the approach to these constants is from below, and does not happen even at $R_9 = 2 fm$, the maximal value shown in the figure.

Finally, we show by a straight line the non-perturbative part of the Cornell potential used in the previous section. The overall force (potential gradient) is quite close to the instanton-induced force.

Using the instanton-induced potentials into the radial Schroedinger equation in the $\bar{3}3$ channel, we have for the s-level splittings

$$\begin{aligned} M(2) - M(1) &\approx 362 MeV \\ M(3) - M(1) &\approx 578 MeV \\ M(4) - M(1) &\approx 657 MeV \end{aligned} \quad (26)$$

The comparison to the empirical splittings in (23), shows satisfactory agreement. We emphasize that the calculation of the radial potential does not involve any free parameters, as we made use of the same instanton ensemble for also the $\bar{q}q$ and qqq channels.

VI. SUMMARY AND DISCUSSION

We conclude, by first recalling some of the questions of hadronic spectroscopy we have tried to address. A central one is the nature of the effective static potential for quarkonia, including the perturbative contribution one-gluon-exchange at short

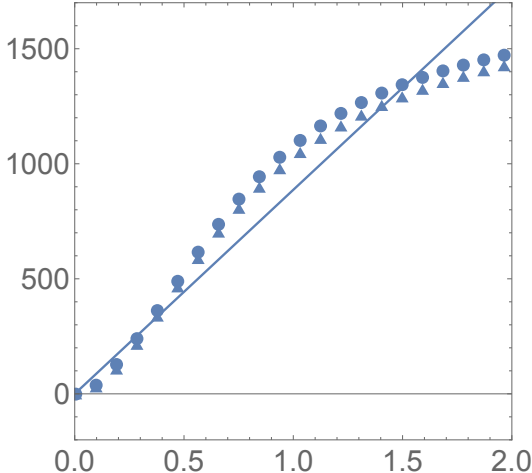


FIG. 8. Four-quark effective static potentials (in MeV) versus the hyperdistance R_9 (in fm), calculated from the correlators of four Wilson lines in tetraquarks. The color indices are connected according to products of color wave functions at $T \rightarrow \pm\infty$ (D4) at times $\pm T \rightarrow \pm\infty$. The results for the $\bar{3}3$ channel are shown by triangles, and that for the $6\bar{6}$ channel by closed points. The line corresponds to the non-perturbative part of the Cornell potential projected to the hyper-distance R_9 , as described in Appendix B.

distance, and the non-perturbative and about linear contribution at large distance. It has approximately the same tension in quarkonia as deduced from Regge trajectories of light mesons and baryons.

In this paper we have addressed the effective interaction potentials in two types of few-body hadrons – baryons and tetraquarks. While for the one-gluon-exchange modifications by color factors can be easily calculated (resulting e.g. in the known factor $\frac{1}{2}$ in baryons), the corresponding factors in the non-perturbative part is quite nontrivial. It is even unclear whether it can or cannot be dominated by a sum of binary interactions.

For simplicity and symmetry, we use the so called “hyperdistance approximation”, projecting the relevant multidimensional potentials to a single radial variable R_6 or R_9 , in the space of Jacobi coordinates. The squared hyper-distances are proportional to the sum of the squares of all the binary distances, in a very symmetric way. Solving radial Schrodinger equation one finds spectra and wave functions, in 6 and 9 dimensions respectively. We focused on the splittings between the subsequent s-shell levels, known to be rather insensitive to the quark masses,

but roughly proportional to the force between the constituents. We found that the Cornell-type potential, averaged over solid angles in these spaces and with proper color factors, does indeed generate reasonable values for $uuu = \Delta^{++}$ baryons, and for the recently discovered all-charm tetraquarks.

The static spin-independent potentials are known to be related to correlators of few (3,4 etc) Wilson lines, connected in ways depending on the external color wave functions of the given hadron. Such objects are very non-local correlators of vacuum fields, with a non-trivial dependence on the locations of the quarks. *A priori* it not possible to use a traditional notion of the potential energy being a sum of binary potentials. For corresponding lattice studies, see e.g. [9] for baryons and [10] for tetraquarks.

The Euclidean gauge fields in the QCD vacuum can be, in a semiclassical approximation, approximated by *instantons*, 4-dimensional solitons (pseudo-particles) describing tunneling events through topological barriers which separate configurations with different Chern-Simons numbers. Models of their ensembles were developed, both using phenomenology of hadronic correlation functions (for review see e.g.[12]) and direct lattice studies of the fields. The instanton fields are special because they are giving simple analytic answers for Wilson lines, and therefore one can derive rather simple analytic expressions for their correlators [15]. Basically, the Wilson lines are certain rotation in the quark color spaces, by an angle that depends on the distance to the instanton center.

In [1] we introduced and used the “dense instanton liquid model” to evaluate static and spin-dependent potentials in quarkonia. In this paper we continue this work, by evaluating the instanton-induced potentials via correlators of Wilson lines, for baryons and tetraquarks.

The instanton-induced potential for baryons is derived in section III B. Somewhat surprisingly, we found that the triple-W correlators can be written as a sum of binary potentials. Furthermore, its shape happens to be the same as for quarkonia, differing just by an overall factor. We think that the main reason for this, is the fact that the instanton fields are always inside a certain $SU(2)$ subspace of the $SU(3)$ color group, while the color wave functions of baryons require that the three quarks carry always three mutually orthogonal colors.

We have evaluated the instanton-induced potential for tetraquarks. In this case the color wave

functions are different. We have considered two options, which we referred to as $\bar{3}3$ and $\bar{6}\bar{6}$ according to their diquark color content. The convolution with four Wilson lines leads to certain diagrams shown in Fig.7. Apparently in this case, no splitting of the 4-body interactions into pairwise binary terms takes place. Yet the effective potentials for the $\bar{3}3$ and $\bar{6}\bar{6}$ channels as a function of the hyperdistance R_9 , shown in Fig.8, are similar in shape to those in quarkonia and qqq cases.

Before we made use of these potentials in spectroscopy, in section II A we returned to the (rather well-studied) case of heavy quarkonia, and in particular to the relation between their spectra and the effective potentials. In order not to deal with the subtleties related to the quark masses and additive terms in the potentials, we focused on the *splittings* between the s-shell levels, using the standard 3-dimensional Schroedinger equation. We have seen that while the Cornell-type linear+Coulomb potentials do a very good job, our instanton-induced potential can also be used, with a precision even better than the fitted Martin potential.

Proceeding to the baryons and tetraquarks, we used a very similar approach, based on the so called "hyper-spherical approximation", or "method of K-harmonics" known since 1960's. It is based on the assumption that the lowest few-body states are "hyper-spherically symmetric", in the 6-dimensional space for baryons, and 9-dimensional space for tetraquarks, in terms of pertinent Jacobi coordinates. Solving the radial hyper-spherical Schroedinger equation, we obtained the spectra, in particular the splittings between s-shell levels. For baryons we did so for the ccc and uuu flavor-symmetric baryons. While the formers are not yet experimentally observed, the latter belong to the family of Δ^{++} for which we found a reasonable agreement between the derived effective potential, and the experimentally observed separations of the (s-shell) states.

In section IV B, following the pioneering paper [4], we applied the hyper-spherical approximation to all-charm tetraquarks. This method assumes that lowest the states are "hyper-spherical" in 9-dimensional space of Jacobi coordinates. The interaction assumed to be the sum of 6 binary potentials of the Cornell type times $\lambda_i^A \lambda_j^A$ color matrices, times some extra effective strength factor. Focusing not on masses themselves, but on the *splittings* between the states, we simplified the problem by

eliminating the overall constants, a conspiracy between quark masses and constants in the potentials. Our instanton-based potentials in $\bar{3}3$ or $\bar{6}\bar{6}$ channels are very close, so in a way we confirmed the conjecture in [4] that they are the same, in spite of certain repulsive terms in the $\bar{6}\bar{6}$ case. Furthermore, this potential leads to $1S - 2S - 3S$ splittings (26) in fair agreement with the observed splittings between the three recently reported resonances (23). We also compared our results to the recent analysis in [24], based on the hyper-distance approximation as well.

Finally, we stress once again that the hyper-radial qqq and $cc\bar{c}\bar{c}$ effective potentials we derived, Figs.5 and 8, originate without change from the instanton model of the QCD vacuum. Its two parameters are fixed by lattice observation of instanton, and therefore one may say that the present paper has *no* free parameters whatsoever. The hadronic masses and wave functions we derived, follow directly from a model of the QCD vacuum.

Acknowledgements:

This work is supported by the Office of Science, U.S. Department of Energy under Contract No. DE-FG-88ER40388.

Appendix A: Hyper-spherical harmonics

The non-relativistic kinetic energy of A particles using N Jacobi coordinates, takes the simple form [25]

$$-\frac{1}{2} \sum_{i=1}^A \nabla_i^2 = -\frac{1}{2} \left(\partial_\rho^2 + \frac{3N-1}{\rho} \partial_\rho - \frac{1}{\rho^2} K_N^2 \right) \quad (\text{A1})$$

The hyper-spherical harmonics (HHs) are the eigenstates of the grand-angular momentum

$$K_N^2 \mathcal{Y}_{[K]}^{KLM_L}(\Omega_N) = (K(K+3N-2)) \mathcal{Y}_{[K]}^{KLM_L}(\Omega_N) \quad (\text{A2})$$

The $2^N + N$ angles $\Omega_N = (\hat{\xi}_1, \dots, \hat{\xi}_N; \varphi_1, \dots, \varphi_N)$, are those of the individual Jacobi coordinates $\hat{\xi}_i$, and the hyperangles $\cos\varphi_j = \xi_j/\rho$. L, M_L are the standard quantum numbers of the total orbital angular momentum L^2, L_z . The specific form of the HHs follows by recoupling the individual angular momenta l_i . They are normalized as

$$\int d\Omega_N \mathcal{Y}_{[K]}^{KLM_L}(\Omega_N) \mathcal{Y}_{[K']}^{K'L'M'_L}(\Omega_N) = \delta_{[K],[K']} \quad (\text{A3})$$

and their total number is [25]

$$d_K = (2K + 3N - 2) \frac{(K + 3N - 3)!}{K!(3N - 2)!} \quad (\text{A4})$$

For instance for $A = 4$ particles with $N = 3$, the $K = 0$ HH has degeneracy $d_0 = 1$, and the $K = 1$ HHs have degeneracy $d_1 = 9$.

Appendix B: Quantum mechanics of three quarks in hyperspherical coordinates

To describe the specifics of the hyper-spherical approximation, we first consider three quarks in a baryon. The three coordinate vectors of the quarks are compressed into two (modified) Jacobi vectors

$$\vec{\rho} = \frac{1}{\sqrt{2}} \vec{r}_{12} \quad \vec{\lambda} = \frac{1}{\sqrt{6}} (\vec{r}_{13} + \vec{r}_{23}) \quad (\text{B1})$$

with $\vec{r}_{ij} = \vec{r}_i - \vec{r}_j$ as 3-dimensional vectors. The 6-dimensional radial coordinate denoted by R_6 is given by

$$R_6^2 = \vec{\rho}^2 + \vec{\lambda}^2 = \frac{1}{3} [(\vec{r}_1 - \vec{r}_2)^2 + (\vec{r}_1 - \vec{r}_3)^2 + (\vec{r}_3 - \vec{r}_2)^2] \quad (\text{B2})$$

so it is related to the sum of all the squared interquark distances, in a symmetric manner. The coefficients in the definitions of these coordinates also ensure that the kinetic energy takes the form of a Laplacian in 6-dimensional space $\{\vec{\rho}, \vec{\lambda}\}$, divided by $2m$. (The total momentum has a different coefficient, but it is presumed to be zero anyway.)

The hyper-spherical approximation in its most symmetric form does not distinguish $\vec{\rho}, \vec{\lambda}$, but treats all 6 coordinates on equal footing. Standard spherical coordinates can be introduced with 5 angles $\theta_1, \theta_2, \theta_3, \theta_4 \in [0, \pi], \phi \in [0, 2\pi]$, and a 6-dimensional solid angle

$$\Omega_6 = \int d\theta_1 d\theta_2 d\theta_3 d\theta_4 d\phi \quad (\text{B3})$$

$$\times \sin(\theta_1)^4 \sin(\theta_2)^3 \sin(\theta_3)^2 \sin(\theta_4) = \pi^3$$

(Alternative a 6-dimensional coordinate space parametrization with five angular variables can be defined as $\vec{\rho} = R_6 \cos(\Phi) \hat{n}_1, \vec{\lambda} = R_6 \sin(\Phi) \hat{n}_2$ with two unit vectors having independent solid angle integrals.)

The effective potential V_6 in general depends on all 6 coordinates, but can be "projected onto the 6-dimensional radial coordinate R_6 " by angular average. If the binary potentials are of Cornell-type, a

combination of linear and inverse terms, e.g. $V_{12} = \kappa_2/r_{12} + \sigma_2 r_{12}$, then their projections are done via the solid angle integral

$$\langle r_{12} \rangle = \sqrt{2} \langle |\vec{\rho}| \rangle = \sqrt{2} R_6 \frac{\int d\Omega_6 d_{12}}{\Omega_6}$$

$$\approx 0.960 R_6 \quad (\text{B4})$$

where

$$d_{12} = \sqrt{C_1^2 + S_1^2 C_2^2 + S_1^2 S_2^2 C_3^2} = \sqrt{1 - S_1 S_2 S_3} \quad (\text{B5})$$

with the short-hand notations $C_i = \cos(\theta_i), S_i = \sin(\theta_i)$.

A similar averaging of the inverse power of r_{12} has $1/\sqrt{2} d_{12}$ in the integral

$$\left\langle \frac{1}{r_{12}} \right\rangle = \frac{1}{\Omega_6} \int d\Omega_6 \frac{1}{\sqrt{2} d_{12}}$$

$$\approx 1.20/R_6 \quad (\text{B6})$$

Note that the convergence of this integral is due to the fact that d_{12} can only vanish if all three angles $\theta_1, \theta_2, \theta_3 \approx \pi/2$. As a result, the effective potential in hyper-spherical coordinate R_6 takes the form

$$V(R_6) = 3 [0.96 * R_6 * (0.113/2) - 1.2 R_6 * (0.64/2)] \quad (\text{B7})$$

where the factor 3 appears due to the inclusion of interactions of 12, 13, 23 quark pairs. The numerical values 0.113, 0.64 (in GeV^2 units) are from our version of the Cornell potential (3), and the division by two comes from assumption of Ansatz A for the $q\bar{q}$ relative to the $\bar{q}q$ potential.

Appendix C: Quantum mechanics of four quarks in hyper-spherical coordinates

The generalized Jacobi coordinates for 4 particles are defined by

$$\vec{\xi}_1 = \sqrt{\frac{1}{2}} (\vec{r}_1 - \vec{r}_2) \quad (\text{C1})$$

$$\vec{\xi}_2 = \sqrt{\frac{1}{6}} (\vec{r}_1 + \vec{r}_2 - 2\vec{r}_3)$$

$$\vec{\xi}_3 = \frac{1}{2\sqrt{3}} (\vec{r}_1 + \vec{r}_2 + \vec{r}_3 - 3\vec{r}_4)$$

In this case the hyper-distance

$$R_9^2 = \vec{\xi}_1^2 + \vec{\xi}_2^2 + \vec{\xi}_3^2 \quad (\text{C2})$$

$$= \frac{1}{4} [(\vec{r}_1 - \vec{r}_2)^2 + (\vec{r}_1 - \vec{r}_3)^2 + (\vec{r}_1 - \vec{r}_4)^2$$

$$+ (\vec{r}_3 - \vec{r}_2)^2 + (\vec{r}_4 - \vec{r}_2)^2 + (\vec{r}_3 - \vec{r}_4)^2]$$

is connected to the sum of the squared distances of all six pairs of quarks. When supplemented by 8 angles, it describes the 9-dimensional space in which quantum mechanics is performed. Again, with the total momentum set to zero, the kinetic energy is given by the 9-dimensional Laplacian with the standard coefficient

$$K = -\frac{1}{2m_c}\Delta_\xi \quad (\text{C3})$$

The corresponding calculations are in section IV B.

(To our surprise, in [24] *non*-Jacobi coordinates are used, namely

$$\vec{\xi}_1 = \sqrt{\frac{1}{2}}(\vec{r}_1 - \vec{r}_2) \quad (\text{C4})$$

$$\vec{\xi}_2 = \frac{1}{2}(\vec{r}_3 + \vec{r}_4 - \vec{r}_1 - \vec{r}_2)$$

$$\vec{\xi}_3 = \sqrt{\frac{1}{2}}(\vec{r}_3 - \vec{r}_4) \quad (\text{C5})$$

for which neither the radial coordinate is the symmetric sum of all distances as above, nor the kinetic energy is the Laplacian.)

The dependence on the hyper-distance only means that we deal with the lowest $K = 0$ or s-shell. Only the radial Schroedinger equation needs to be solved. Note that after changing to the reduced wavefunction, it differs from the familiar 3-dimensional case, by only the ‘‘quasi-centrifugal’’ term $12/R_9^2$.

The angular averaging is performed as in the previous section, except now there is a different volume element, namely

$$\begin{aligned} \Omega_9 &= \int \left(\prod_{i=1}^7 d\theta_i \right) d\phi \quad (\text{C6}) \\ &\times \sin(\theta_1)^7 * \sin(\theta_2)^6 * \sin(\theta_3)^5 * \sin(\theta_4)^4 \\ &\times \sin(\theta_5)^3 * \sin(\theta_6)^2 * \sin(\theta_7) = \frac{32\pi^4}{105} \end{aligned}$$

The angular integrations when averaging using the Cornell potential, are done as in the previous section, with obvious changes

$$\begin{aligned} \langle r_{12} \rangle &= \sqrt{2}\langle |\vec{\rho}| \rangle = \frac{\sqrt{2}R_9}{\Omega_9} \int d\Omega_9 d_{12} \\ &\approx 0.773R_9 \quad (\text{C7}) \end{aligned}$$

$$\begin{aligned} \left\langle \frac{1}{r_{12}} \right\rangle &= \frac{1}{R_9\Omega_9} \int \frac{d\Omega_9}{\sqrt{2}d_{12}} \\ &\approx 1.55/R_9 \quad (\text{C8}) \end{aligned}$$

Appendix D: All-charm tetraquarks

1. Color-spin wave functions

The natural way to define the wave function of the $\bar{c}ccc$ tetraquark, is to start with cc and $\bar{c}\bar{c}$ diquarks. Fermi symmetry requires wave functions to be antisymmetric under quark permutations, leaving two possibilities

$$color = [\bar{3}] \text{ (antysym)}, \quad spin = 1 \text{ (sym)} \quad (\text{D1})$$

$$color = [6] \text{ (sym)}, \quad spin = 0 \text{ (antisym)} \quad (\text{D2})$$

The total color is zero, and therefore the wave function should take the form

$$\psi = F_{\bar{3}\bar{3}}(\xi_i)C_{\bar{3}\bar{3}}(c_i)S_1(s_i) + F_{6\bar{6}}(\xi_i)C_{6\bar{6}}(c_i)S_0(s_i) \quad (\text{D3})$$

where the two spatial wave functions F depend in general on 9 Jacobi coordinates, $C(c_i), i = 1..4$, on color indices, and $S(s_i), i = 1..4$ quark spin variables. If particles 1,2 are quarks and 3,4 antiquarks, one can define the color and spin structures as

$$\begin{aligned} C_{\bar{3}\bar{3}}(c_1c_2c_3c_4) &= \sum_c \epsilon_{c_1,c_2,c} \epsilon_{c_3,c_4,c} / \sqrt{12} \quad (\text{D4}) \\ &= (\delta_{c_1c_3} \delta_{c_2c_4} - \delta_{c_1c_4} \delta_{c_2c_3}) / \sqrt{12} \\ C_{6\bar{6}}(c_1c_2c_3c_4) &= (\delta_{c_1c_3} \delta_{c_2c_4} + \delta_{c_1c_4} \delta_{c_2c_3}) / \sqrt{24} \\ S_0 &= (\uparrow\downarrow - \downarrow\uparrow) / \sqrt{2} \\ S_1 &= (\uparrow\downarrow + \downarrow\uparrow) / \sqrt{2} \end{aligned}$$

with the normalization

$$\langle \psi | \psi \rangle = \int d^9\xi |F_{\bar{3}\bar{3},6\bar{6}}|^2 \quad (\text{D5})$$

Note that, while the color structures in (D3) are not orthogonal to each other, the spin structures are. So, neglecting the spin-dependent forces (small for charm quarks), we expect the Hamiltonian to be diagonal, in terms of $F_{\bar{3}\bar{3}}, F_{6\bar{6}}$.

Following [4], we assume the color dependence of the forces to be similar to those from one-gluon-exchange, namely

$$V = \sum_{i>j} w_{ij}(r_{ij}) \sum_{A=1,8} \frac{1}{4} \lambda_i^A \lambda_j^A \quad (\text{D6})$$

The lower indices of Gell-Mann matrices indicate on which quark color index they act.

An additional condition is that for antiquarks (3,4 in current setting), we have to conjugate

$$\lambda^A \rightarrow \tilde{\lambda}^A = -\lambda^{A*}$$

whereby five contributions change sign and three do not. Averaging V over ψ explicitly, and summing

over all indices (we did it using Mathematica) we obtained two expressions (which agree with those in [4])

$$\langle \psi | V | \rangle = \left[\begin{array}{l} -\frac{1}{3} F_{33}^2 (w_{13} + w_{14} + w_{24} + w_{32} + 2w_{12} + 2w_{34}), \\ -\frac{1}{6} F_{66}^2 (-2w_{12} - 2w_{34} + 5w_{24} + 5w_{13} + 5w_{32} + 5w_{14}) \end{array} \right]$$

Note that in the $6\bar{6}$ channel, there are repulsive quark-quark contributions. Furthermore, *assuming* that all w_{ij} are the same, one arrives at the conclusion in [4], namely that under these assumptions both color-spin tetraquark structures have *the same* interactions. It is *twice* stronger than in the $Q\bar{Q}$ channel (while including all six i, j pairs).

Appendix E: Averaging four Wilson lines over the $SU(3)$ rotations

In this appendix we present expressions for 8 $SU(N_c)$ matrices, averaged over the invariant Haar measure. We do not use them in this paper, since both for the qqq and $qq\bar{q}\bar{q}$ cases considered it turned out that the color wave functions are such that these complicated formulae are not needed. Yet they would be needed for four Wilson lines with arbitrary colors. Since we derived such formulae anyway, we decided to show them in this appendix.

1. Weingarten-style formula

One way to carry the color averaging over four pairs of unitary matrices can be carried using the Weingarten method, producing the following expressions

$$\begin{aligned} & \left\langle U_{c_1}^{a_1} U_{d_1}^{\dagger b_1} U_{c_2}^{a_2} U_{d_2}^{\dagger b_2} U_{c_3}^{a_3} U_{d_3}^{\dagger b_3} U_{c_4}^{a_4} U_{d_4}^{\dagger b_4} \right\rangle_U = \\ & + \frac{6 - 8N_c^2 + N_c^4}{N_c^2(N_c^2 - 1)(N_c^2 - 4)(N_c^2 - 9)} \sum_{n=1}^{4!} \delta_{P_n(d_1 d_2 d_3 d_4)}^{a_1 a_2 a_3 a_4} \delta_{P_n(b_1 b_2 b_3 b_4)}^{c_1 c_2 c_3 c_4} \\ & + \frac{4N_c - N_c^3}{N_c^2(N_c^2 - 1)(N_c^2 - 4)(N_c^2 - 9)} \sum_{n=1}^{4!} \delta_{P_n(d_1 d_2 d_3 d_4)}^{a_1 a_2 a_3 a_4} \\ & \quad \times \left(\delta_{P_n(b_2 b_1 b_3 b_4)}^{c_1 c_2 c_3 c_4} + \delta_{P_n(b_1 b_3 b_2 b_4)}^{c_1 c_2 c_3 c_4} + \delta_{P_n(b_1 b_2 b_4 b_3)}^{c_1 c_2 c_3 c_4} + \delta_{P_n(b_4 b_2 b_3 b_1)}^{c_1 c_2 c_3 c_4} + \delta_{P_n(b_1 b_4 b_3 b_2)}^{c_1 c_2 c_3 c_4} + \delta_{P_n(b_3 b_2 b_1 b_4)}^{c_1 c_2 c_3 c_4} \right) \\ & + \frac{6 + N_c^2}{N_c^2(N_c^2 - 1)(N_c^2 - 4)(N_c^2 - 9)} \sum_{n=1}^{4!} \delta_{P_n(d_1 d_2 d_3 d_4)}^{a_1 a_2 a_3 a_4} \left(\delta_{P_n(b_2 b_1 b_4 b_3)}^{c_1 c_2 c_3 c_4} + \delta_{P_n(b_3 b_4 b_1 b_2)}^{c_1 c_2 c_3 c_4} + \delta_{P_n(b_4 b_3 b_2 b_1)}^{c_1 c_2 c_3 c_4} \right) \\ & + \frac{-3 + 2N_c^2}{N_c^2(N_c^2 - 1)(N_c^2 - 4)(N_c^2 - 9)} \sum_{n=1}^{4!} \delta_{P_n(d_1 d_2 d_3 d_4)}^{a_1 a_2 a_3 a_4} \\ & \quad \times \left(\delta_{P_n(b_2 b_3 b_1 b_4)}^{c_1 c_2 c_3 c_4} + \delta_{P_n(b_1 b_3 b_4 b_2)}^{c_1 c_2 c_3 c_4} + \delta_{P_n(b_3 b_2 b_4 b_1)}^{c_1 c_2 c_3 c_4} + \delta_{P_n(b_2 b_4 b_3 b_1)}^{c_1 c_2 c_3 c_4} + \delta_{P_n(b_1 b_4 b_2 b_3)}^{c_1 c_2 c_3 c_4} + \delta_{P_n(b_3 b_1 b_2 b_4)}^{c_1 c_2 c_3 c_4} + \delta_{P_n(b_4 b_1 b_3 b_2)}^{c_1 c_2 c_3 c_4} + \delta_{P_n(b_4 b_2 b_1 b_3)}^{c_1 c_2 c_3 c_4} \right) \\ & + \frac{-5N_c}{N_c^2(N_c^2 - 1)(N_c^2 - 4)(N_c^2 - 9)} \sum_{n=1}^{4!} \delta_{P_n(d_1 d_2 d_3 d_4)}^{a_1 a_2 a_3 a_4} \\ & \quad \times \left(\delta_{P_n(b_2 b_3 b_4 b_1)}^{c_1 c_2 c_3 c_4} + \delta_{P_n(b_4 b_1 b_2 b_3)}^{c_1 c_2 c_3 c_4} + \delta_{P_n(b_2 b_4 b_1 b_3)}^{c_1 c_2 c_3 c_4} + \delta_{P_n(b_3 b_1 b_4 b_2)}^{c_1 c_2 c_3 c_4} + \delta_{P_n(b_3 b_4 b_2 b_1)}^{c_1 c_2 c_3 c_4} + \delta_{P_n(b_4 b_3 b_1 b_2)}^{c_1 c_2 c_3 c_4} \right) \end{aligned} \tag{E1}$$

In the large N_c limit, it simplifies considerably with the result

$$\left\langle U_{c_1}^{a_1} U_{d_1}^{\dagger b_1} U_{c_2}^{a_2} U_{d_2}^{\dagger b_2} U_{c_3}^{a_3} U_{d_3}^{\dagger b_3} U_{c_4}^{a_4} U_{d_4}^{\dagger b_4} \right\rangle_U = \frac{1}{N_c^4} \sum_{n=1}^{4!} \delta_{P_n(d_1 d_2 d_3 d_4)}^{a_1 a_2 a_3 a_4} \delta_{P_n(b_1 b_2 b_3 b_4)}^{c_1 c_2 c_3 c_4} + \mathcal{O}\left(\frac{1}{N_c^5}\right) \quad (\text{E2})$$

We are using the shorthand notation

$$\sum_{n=1}^{4!} \delta_{P_n(d_1 d_2 d_3 d_4)}^{a_1 a_2 a_3 a_4} \delta_{P_n(b_1 b_2 b_3 b_4)}^{c_1 c_2 c_3 c_4} = \left(\delta_{d_1}^{a_1} \delta_{d_2}^{a_2} \delta_{d_3}^{a_3} \delta_{d_4}^{a_4} \delta_{b_1}^{c_1} \delta_{b_2}^{c_2} \delta_{b_3}^{c_3} \delta_{b_4}^{c_4} + \text{perm.} \right) \quad (\text{E3})$$

where the sum is over the $4!$ P_n elements of the permutation group S_4 , which are explicitly

$$\begin{aligned} P_1(a_1 a_2 a_3 a_4) &= (a_1 a_2 a_3 a_4) \\ P_2(a_1 a_2 a_3 a_4) &= (a_1 a_2 a_4 a_3) \\ P_3(a_1 a_2 a_3 a_4) &= (a_1 a_3 a_2 a_4) \\ P_4(a_1 a_2 a_3 a_4) &= (a_1 a_3 a_4 a_2) \\ P_5(a_1 a_2 a_3 a_4) &= (a_1 a_4 a_2 a_3) \\ P_6(a_1 a_2 a_3 a_4) &= (a_1 a_2 a_3 a_4) \\ P_7(a_1 a_2 a_3 a_4) &= (a_1 a_4 a_3 a_2) \end{aligned}$$

$$\begin{aligned} P_8(a_1 a_2 a_3 a_4) &= (a_2 a_1 a_3 a_4) \\ P_9(a_1 a_2 a_3 a_4) &= (a_2 a_1 a_4 a_3) \\ P_{10}(a_1 a_2 a_3 a_4) &= (a_2 a_3 a_1 a_4) \\ P_{11}(a_1 a_2 a_3 a_4) &= (a_2 a_3 a_4 a_1) \\ P_{12}(a_1 a_2 a_3 a_4) &= (a_2 a_4 a_1 a_3) \\ P_{13}(a_1 a_2 a_3 a_4) &= (a_2 a_4 a_3 a_1) \end{aligned}$$

$$\begin{aligned} P_{14}(a_1 a_2 a_3 a_4) &= (a_3 a_1 a_2 a_4) \\ P_{15}(a_1 a_2 a_3 a_4) &= (a_3 a_1 a_4 a_2) \\ P_{16}(a_1 a_2 a_3 a_4) &= (a_3 a_2 a_4 a_1) \\ P_{17}(a_1 a_2 a_3 a_4) &= (a_3 a_4 a_1 a_2) \\ P_{18}(a_1 a_2 a_3 a_4) &= (a_3 a_4 a_2 a_1) \end{aligned}$$

$$\begin{aligned} P_{19}(a_1 a_2 a_3 a_4) &= (a_4 a_1 a_2 a_3) \\ P_{20}(a_1 a_2 a_3 a_4) &= (a_4 a_1 a_3 a_2) \\ P_{21}(a_1 a_2 a_3 a_4) &= (a_4 a_2 a_1 a_3) \\ P_{22}(a_1 a_2 a_3 a_4) &= (a_4 a_2 a_3 a_1) \\ P_{23}(a_1 a_2 a_3 a_4) &= (a_4 a_3 a_1 a_2) \\ P_{24}(a_1 a_2 a_3 a_4) &= (a_4 a_3 a_2 a_1) \end{aligned} \quad (\text{E4})$$

Note that coefficients have different powers of $1/N_c$, so when $N_c \rightarrow \infty$ the only one left is the first row. However at $N_c = 3$ they are all identical (by modulus) and have alternating signs, so they conspire to cancel. At the other hand, coefficients have $1/(N_c^2 - 9)$ factors prohibiting direct usage of these expressions when $N_c = 3$ (or smaller), without investigations of those cancellations. Clearly, the result (E1) is useful for numerical implementation for $N_c > 3$. For $N_c \leq p = 4$ we now provide alternative and finite identities.

2. Creutz formula

Another way to carry the color averaging in (E1) which is pole free, is by determinantal reduction. More specifically, we will use Creutz's identities [26]

$$\left\langle \prod_{i=1}^{N_c} U_{c_i}^{a_i} \right\rangle_U = \frac{1}{N_c!} \epsilon^{a_1 \dots a_{N_c}} \epsilon_{c_1 \dots c_{N_c}} \quad (\text{E5})$$

and

$$\begin{aligned} U_c^{\dagger a} &= \frac{1}{(N_c - 1)!} \\ &\times \epsilon^{a a_1 \dots a_{N_c-1}} \epsilon_{c c_1 \dots c_{N_c-1}} U_{c_1}^{a_1} \dots U_{c_{N_c-1}}^{a_{N_c-1}} \end{aligned} \quad (\text{E6})$$

where $\epsilon^{a_1 \dots a_{N_c}}$ is the Levi-Cevita tensor of rank- N_c , with $\epsilon^{1 \dots N_c} = 1$.

With this in mind, we can substitute (E6) for the $p = 4$ string of U^\dagger in (E1), with the result

$$\begin{aligned} & \left\langle U_{c_1}^{a_1} U_{d_1}^{\dagger b_1} U_{c_2}^{a_2} U_{d_2}^{\dagger b_2} U_{c_3}^{a_3} U_{d_3}^{\dagger b_3} U_{c_4}^{a_4} U_{d_4}^{\dagger b_4} \right\rangle_U = \\ & \frac{1}{((N_c - 1)!)^{p=4}} \prod_{m=1}^{p=4} \epsilon^{b_m b_{1m} \dots b_{(N_c-1)m}} \epsilon_{d_m d_{1m} \dots d_{(N_c-1)m}} \left\langle \prod_{m=1}^{p=4} U_{c_m}^{a_m} U_{d_{1m}}^{b_{1m}} \dots U_{d_{(N_c-1)m}}^{b_{(N_c-1)m}} \right\rangle_U \end{aligned} \quad (\text{E7})$$

Each of the product is composed rank- N_c Levi-Cevita tensors. The last unitary averaging in (E7) can be undone by the determinantal identity (E5)

$$\begin{aligned} & \left\langle U_{c_1}^{a_1} U_{d_1}^{\dagger b_1} U_{c_2}^{a_2} U_{d_2}^{\dagger b_2} U_{c_3}^{a_3} U_{d_3}^{\dagger b_3} U_{c_4}^{a_4} U_{d_4}^{\dagger b_4} \right\rangle_U = \left(\frac{1}{((N_c - 1)!)^p} \frac{2! \dots (N_c - 1)!}{(p + 1)! \dots (p + N_c - 1)!} \right)_{p=4} \\ & \prod_{m=1}^{p=4} \epsilon^{a_m b_{1m} \dots b_{(N_c-1)m}} \epsilon_{c_m d_{1m} \dots d_{(N_c-1)m}} \left(\prod_{m=1}^{p=4} \epsilon^{a_m b_{1m} \dots b_{(N_c-1)m}} \epsilon_{c_m d_{1m} \dots d_{(N_c-1)m}} + \text{perm.} \right) \end{aligned} \quad (\text{E8})$$

The combinatorial pre-factor follows from the fact that the group integration is invariant under the permutation of the U-factors, with a total of $(pN_c)!$ permutations. Note that many permutations are identical, with only $\frac{(pN_c)!}{(p!(N_c!)^p)}$ independent ones. Clearly all coefficients in (E8) are finite for any value of N_c , in contrast to (E1). We note that (E8) holds for the averaging of even higher products $(UU^\dagger)^p$, and is free of poles whatever p, N_c .

Appendix F: CNZ formula

Finally, another alternative formula for the color averaging can be obtained by using the graphical color projection rules developed in CNZ paper [5]. More specifically, the color averaging $(UU^\dagger)^4$ with $p = 4$, can be tied recursively to $p = 3$ by reduction

$$\begin{aligned} & \left\langle U_{c_1}^{a_1} U_{d_1}^{\dagger b_1} U_{c_2}^{a_2} U_{d_2}^{\dagger b_2} U_{c_3}^{a_3} U_{d_3}^{\dagger b_3} U_{c_4}^{a_4} U_{d_4}^{\dagger b_4} \right\rangle_U = \\ & + \left(\left[\frac{1}{N_c} \delta_{d_1}^{a_1} \delta_{c_1}^{b_1} \mathbf{1}_1 \right] \left\langle U_{c_2}^{a_2} U_{d_2}^{\dagger b_2} U_{c_3}^{a_3} U_{d_3}^{\dagger b_3} U_{c_4}^{a_4} U_{d_4}^{\dagger b_4} \right\rangle_U + \text{perm.} \right) \\ & + \left(([\lambda_1^A]_{d_1}^{a_1} [\lambda_2^B]_{d_2}^{a_2} [\lambda_3^C]_{d_3}^{a_3} [\lambda_4^D]_{d_4}^{a_4}) ([\lambda_1^I]_{c_1}^{b_1} [\lambda_2^J]_{c_2}^{b_2} [\lambda_3^K]_{c_3}^{b_3} [\lambda_4^L]_{c_4}^{b_4}) X^{ABCD} X^{IJKL} \right) \end{aligned} \quad (\text{F1})$$

with the color factors

$$\begin{aligned} X^{ABCD} = & \frac{1}{16(N_c^2 - 1)^2} (\delta^{AB} \delta^{CD} + \delta^{AC} \delta^{BD} + \delta^{AD} \delta^{BC}) \\ & + \frac{1}{4(N_c^2 - 1)} \frac{N_c^2}{4(N_c^2 - 4)^2} (d^{ABM} d^{CDM} + d^{ACM} d^{BDM} + d^{ADM} d^{BCM}) \\ & + \frac{1}{4(N_c^2 - 1)} \frac{1}{4N_c^2} (f^{ABM} f^{CDM} + f^{ACM} f^{BDM} + f^{ADM} f^{BCM}) \\ & + \frac{1}{4(N_c^2 - 1)} \frac{1}{4(N_c^2 - 4)} (d^{ABM} f^{CDM} + d^{ACM} f^{BDM} + d^{ADM} f^{BCM}) \\ & + \frac{1}{4(N_c^2 - 1)} \frac{1}{4(N_c^2 - 4)} (f^{ABM} d^{CDM} + f^{ACM} d^{BDM} + f^{ADM} d^{BCM}) \end{aligned} \quad (\text{F2})$$

and similarly for X^{IJKL} . The reduced averaging over $(UU^\dagger)^3$ gives

$$\begin{aligned}
\left\langle U_{c_2}^{a_2} U_{d_2}^{\dagger b_2} U_{c_3}^{a_3} U_{d_3}^{\dagger b_3} U_{c_4}^{a_4} U_{d_4}^{\dagger b_4} \right\rangle_U &= \left[\frac{1}{N_c} \delta_{d_2}^{a_2} \delta_{c_2}^{b_2} \mathbf{1}_2 \right] \left[\frac{1}{N_c} \delta_{d_3}^{a_3} \delta_{c_3}^{b_3} \mathbf{1}_3 \right] \left[\frac{1}{N_c} \delta_{d_4}^{a_4} \delta_{c_4}^{b_4} \mathbf{1}_4 \right] \\
&+ \left(\left[\frac{1}{N_c} \delta_{d_2}^{a_2} \delta_{c_2}^{b_2} \mathbf{1}_2 \right] \left[\frac{1}{4(N_c^2 - 1)} [\lambda_3^A]_{d_3}^{a_3} [\lambda_4^A]_{d_4}^{a_4} [\lambda_3^B]_{c_3}^{b_3} [\lambda_4^B]_{c_4}^{b_4} \right] + 2 \text{ perm.} \right) \\
&+ \frac{N_c}{8(N_c^2 - 1)(N_c^2 - 4)} \left[d^{ABC} [\lambda_2^A]_{d_2}^{a_2} [\lambda_3^B]_{d_3}^{a_3} [\lambda_4^C]_{d_4}^{a_4} \right] \left[d^{IJK} [\lambda_2^I]_{c_2}^{b_2} [\lambda_3^J]_{c_3}^{b_3} [\lambda_4^K]_{c_4}^{b_4} \right] \\
&+ \frac{1}{8N_c(N_c^2 - 1)} \left[f^{ABC} [\lambda_2^A]_{d_2}^{a_2} [\lambda_3^B]_{d_3}^{a_3} [\lambda_4^C]_{d_4}^{a_4} \right] \left[f^{IJK} [\lambda_2^I]_{c_2}^{b_2} [\lambda_3^J]_{c_3}^{b_3} [\lambda_4^K]_{c_4}^{b_4} \right] \tag{F3}
\end{aligned}$$

-
- [1] E. Shuryak and I. Zahed, *Phys. Rev. D* **107**, 034023 (2023), [arXiv:2110.15927 \[hep-ph\]](#).
- [2] Y. A. Simonov, *Sov. J. Nucl. Phys.* **3**, 461 (1966).
- [3] E. Shuryak and J. M. Torres-Rincon, *Phys. Rev. C* **100**, 024903 (2019), [arXiv:1805.04444 \[hep-ph\]](#).
- [4] A. M. Badalian, B. L. Ioffe, and A. V. Smilga, *Nucl. Phys. B* **281**, 85 (1987).
- [5] S. Chernyshev, M. A. Nowak, and I. Zahed, *Phys. Rev. D* **53**, 5176 (1996), [arXiv:hep-ph/9510326](#).
- [6] M. Ferraris, M. M. Giannini, M. Pizzo, E. Santopinto, and L. Tiator, *Phys. Lett. B* **364**, 231 (1995).
- [7] K. Gandhi, Z. Shah, and A. K. Rai, *Eur. Phys. J. Plus* **133**, 512 (2018), [arXiv:1811.00251 \[hep-ph\]](#).
- [8] N. Brambilla *et al.*, (2022), [arXiv:2203.16583 \[hep-ph\]](#).
- [9] Y. Koma and M. Koma, *Phys. Rev. D* **95**, 094513 (2017), [arXiv:1703.06247 \[hep-lat\]](#).
- [10] P. Bicudo, M. Cardoso, O. Oliveira, and P. J. Silva, *Phys. Rev. D* **96**, 074508 (2017), [arXiv:1702.07789 \[hep-lat\]](#).
- [11] E. V. Shuryak, *Nucl. Phys. B* **203**, 93 (1982).
- [12] T. Schäfer and E. V. Shuryak, *Rev. Mod. Phys.* **70**, 323 (1998), [arXiv:hep-ph/9610451](#).
- [13] R. L. Workman *et al.* (Particle Data Group), *PTEP* **2022**, 083C01 (2022).
- [14] H. Grosse and A. Martin, *Phys. Rept.* **60**, 341 (1980).
- [15] C. G. Callan, Jr., R. F. Dashen, D. J. Gross, F. Wilczek, and A. Zee, *Phys. Rev. D* **18**, 4684 (1978).
- [16] E. Shuryak and I. Zahed, *Phys. Rev. D* **107**, 034024 (2023), [arXiv:2111.01775 \[hep-ph\]](#).
- [17] E. Shuryak and I. Zahed, (2021), [arXiv:2112.15586 \[hep-ph\]](#).
- [18] A. B. Guimarães, H. T. Coelho, and R. Chanda, *Phys. Rev. D* **24**, 1343 (1981).
- [19] R. Aaij *et al.* (LHCb), *Sci. Bull.* **65**, 1983 (2020), [arXiv:2006.16957 \[hep-ex\]](#).
- [20] J. Zhang and K. Yi (CMS), *PoS ICHEP2022*, 775 (2022), [arXiv:2212.00504 \[hep-ex\]](#).
- [21] Y. Xu (ATLAS), *Acta Phys. Polon. Supp.* **16**, 21 (2023), [arXiv:2209.12173 \[hep-ex\]](#).
- [22] M. Karliner and J. L. Rosner, *Phys. Rev. D* **102**, 114039 (2020), [arXiv:2009.04429 \[hep-ph\]](#).
- [23] J. F. Giron and R. F. Lebed, *Phys. Rev. D* **102**, 074003 (2020), [arXiv:2008.01631 \[hep-ph\]](#).
- [24] A. M. Badalian, (2023), [arXiv:2305.04585 \[hep-ph\]](#).
- [25] M. Fabre de la Ripelle and J. Navarro, *Annals of Physics* **123**, 185 (1979).
- [26] M. Creutz, *J. Math. Phys.* **19**, 2043 (1978).